

Mahajan

Adaptive optics without wavefront sensors

Virendra N. Mahajan, Jacques Govignon, Ricky J. Morgan
The Charles Stark Draper Laboratory, Inc., Cambridge, Massachusetts 02139

Abstract

Two sharpness functions are considered for the problem of dynamic phase estimation and correction of aberrated images. One is based on the integral of the square of the image irradiance distribution. The other uses integration of the irradiance distribution over an area smaller than the diffraction-limited resolution area. Examples of phase retrieval using these sharpness functions are given, and laboratory experiments on their verification are described. Applications of this technique to high-energy laser systems, thermal blooming, imaging through atmospheric turbulence, and large optical systems are discussed.

Introduction

An adaptive optical imaging system generally consists of an imaging element, a sensor for determining the wavefront errors of an image forming wave, and an adaptive element (corrector) to compensate for these errors. In this paper we use image sharpness functions¹ for adaptive estimation and correction of aberrations of an incoherent optical imaging system. An aberrated image is corrected by introducing aberrations into an adaptive element until a sharpness function, which is derived from the image irradiance data, is optimized. The sharpness functions have the property that they achieve their extremum values when the image is aberration free. Thus, by forming a closed loop between the image and the adaptive element, an aberration-free image is obtained without the use of any pupil-plane wavefront sensor. This method can also be used for phase retrieval of aberrated images.

Two sharpness functions are considered for the problem of phase estimation and correction of degraded images. One is based on the integral of the square of the image irradiance distribution. The other uses integration of the irradiance distribution over a small area, i.e., it is a measure of the encircled energy of a point-spread function. Examples of phase retrieval using these sharpness functions are given, and laboratory experiments on their verification are described. Applications of this technique to high-energy laser systems, thermal blooming, imaging through atmospheric turbulence, and large optical systems are discussed.

Image sharpness functions

If $I(\vec{r})$ represents the irradiance distribution of an image for a given shape of the pupil and amplitude distribution across it, then the sharpness functions

$$S_1 = \int I^2(\vec{r}) d\vec{r} \quad (1)$$

and

$$S_2 = \int_{\Delta\vec{r}} I(\vec{r}) d\vec{r} \quad (2)$$

considered as functions of aberrations are maximum for an aberration-free image. Whereas in Eq. (1) the integration is carried out over the incoherent image of an isoplanatic extended object with a uniform background, in Eq. (2) it is carried out over a small region of the image of a point (i.e., unresolved) object. The sharpness function S_2 is sensitive to a wavefront tilt, but S_1 is not. Therefore, when using S_1 , the motion of an image is corrected separately, e.g., by centroid detection and a tilt-control mirror. It is evident that, in practice, the use of S_1 requires sampling of the image by an array of small detectors.

Figure 1 shows how S_1 and S_2 vary, for example, with balanced spherical aberration for a point object. The spherical aberration is balanced with an equal and opposite amount of defocus to yield a minimum variance. The region of integration of the point spread function is a square with a full width of $2\lambda F$, where λ is the optical wavelength and F is the focal ratio (f-number) of the image. It is evident from this figure that when the aberration is large, not only does the sensitivity of the sharpness functions decrease, but also, that they do not necessarily increase with a decrease in the amount of aberration. A similar behavior is found for the other primary aberrations.

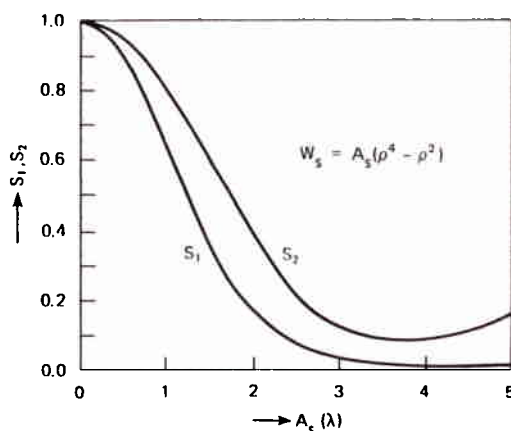


Figure 1. Variation of sharpness functions S_1 and S_2 with balanced spherical aberration.

The problem of sampling the image can be avoided in the case of known extended objects if a mask that has a transmission which is proportional to its unaberrated image irradiance distribution $I_0(\vec{r})$ is placed over a large single detector. Thus, the detector signal given by the sharpness function

$$S_3 = \int I(\vec{r}) I_0(\vec{r}) d\vec{r} \quad (3)$$

is maximized when the aberrations are zero. Its maximum value is equal to that of S_1 . Another possibility is the use of the sharpness function

$$S_4 = \int [I(\vec{r}) - I_0(\vec{r})]^2 d\vec{r} \quad (4)$$

which has a minimum value of zero when the aberrations are zero. In this case no mask is needed, but again, the image has to be sampled. Both S_3 and S_4 are sensitive to a wavefront tilt.

A comparison of the various sharpness functions is given in Table 1. Note that whenever the image must be sampled, a detector array is used and therefore, more data processing is required. Accordingly, the rate of aberration correction will be lower.

Table 1. Comparison of the Various Sharpness Functions

Sharpness Function	Object	Detector	Bandwidth of Correction	Sensitivity to Tilt
$S_1 = \int I^2 d\vec{r}$	Point, extended	Array	Low	No
$S_2 = \int_{\Delta\vec{r}} I d\vec{r}$	Point	Single	High	Yes
$S_3 = \int I I_0 d\vec{r}$	Point, known extended	Single	High	Yes
$S_4 = \int (I - I_0)^2 d\vec{r}$	Point, known extended	Array	Low	Yes

Phase retrieval

Consider an imaging system with a circular pupil of unit radius aberrated by an aberration given by

$$W(\rho, \theta) = A_t \rho \cos \theta + B_t \rho \sin \theta + A_d \rho^2 + A_a \rho^2 \cos 2\theta + B_a \rho^2 \sin 2\theta + A_c \rho^3 \cos \theta + B_c \rho^3 \sin \theta + A_s \rho^4 \quad (5)$$

ADAPTIVE OPTICS WITHOUT WAVEFRONT SENSORS

where $0 < \rho < 1$ and $0 < \theta < 2\pi$. Thus the aberration function is made up of tilt (A_t, B_t), defocus A_d , astigmatism (A_a, B_a), coma (A_c, B_c), and spherical aberration A_s . We have considered several combinations of these aberration coefficients such that the peak-to-peak value of the aberration function is $\leq 2\lambda$. As an example, let $A_t = -0.376$, $B_t = -0.432$, $A_d = -0.110$, $A_a = 0.354$, $B_a = 0.338$, $A_c = 0.564$, $B_c = 0.648$, and $A_s = 0.636$ where all of the coefficients are in units of the optical wavelength. For simplicity, the amount of coma chosen is such that when combined with the tilt, it gives a minimum aberration variance. A plot of the aberration function and the corresponding point-spread function (PSF) are shown in Figure 2. The peak-to-peak value of the aberration, Strehl ratio, and sharpness value of the image are also given in the figure.

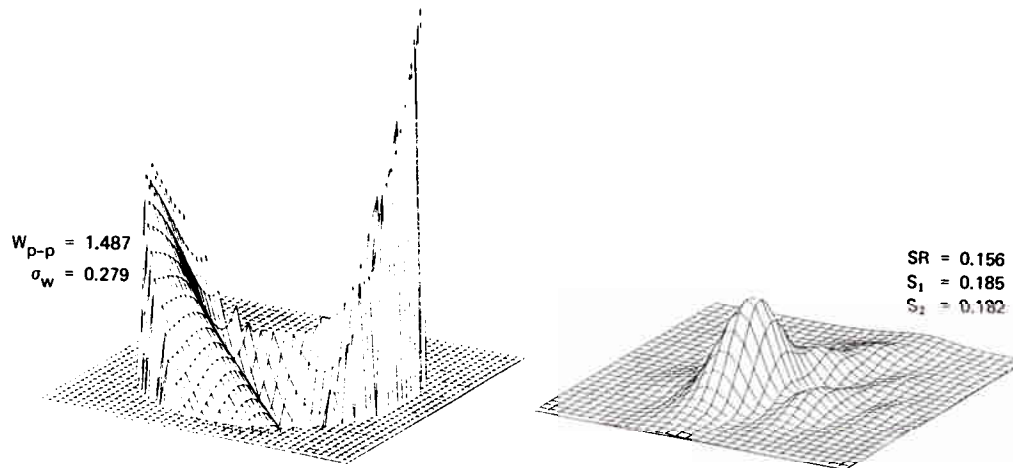


Figure 2. Aberration function and the aberrated image. The peak-to-peak value (W_{p-p}) and the standard deviation (σ_w) of the aberration are given in units of λ . The Strehl ratio (SR) and the image sharpness values S_1 and S_2 are also given.

In our phase retrieval algorithm,² aberrations are introduced sequentially in terms of orthonormal Zernike polynomials³ $\epsilon_m \sqrt{2(n+1)} R_n^m(\rho) \begin{matrix} \cos m\theta \\ \sin m\theta \end{matrix}$, where $\epsilon_m = 1/\sqrt{2}$ when $m = 0$ and $\epsilon_m = 1$ when $m \neq 0$. As a small amount of aberration is introduced, the sharpness function is evaluated, and depending on the change from its previous value, more aberration with positive or negative sign is introduced. From the original and the two new values of the sharpness function, the required amount of correction of that aberration is estimated and a correction is made. This procedure is repeated for each of the polynomial aberrations in the algorithm, and the whole process is repeated iteratively. In practice, the aberrations may be introduced sequentially or in parallel depending upon the bandwidth requirement and affordable complexity. For parallel operation, the aberrations may be introduced with a different harmonic dependence on time for each polynomial aberration, so that their effects on the sharpness function can be discerned.

Figures 3 and 4 show the progression of phase retrieval and image correction using sharpness functions S_1 and S_2 , respectively. Both the residual aberration function and the corresponding PSFs are shown in these figures. An iteration in these figures is defined to be one pass through all the polynomial aberrations. It is evident from these figures that both sharpness functions lead to an excellent correction of the image in two iterations. The region of integration for calculating S_2 in this example was a square with a full width equal to the radius of the Airy disc.

Experimental verifications

A schematic of the laboratory setup for testing the use of sharpness functions in a closed-loop manner is shown in Figure 5. To simulate a point object, a pinhole is illuminated by a He-Ne laser beam. The light from this object falls on a deformable membrane mirror fabricated by the Perkin-Elmer Corporation.⁴ The part of the optical train between the laser and the deformable mirror can also be looked upon as a beam expander. The figure of the membrane is controlled electrostatically by a set of 52 actuators distributed over an area approximately 1 inch in diameter. We wired the actuators in such a way that the membrane figure can be controlled in terms of Zernike modes. When the controller is off,

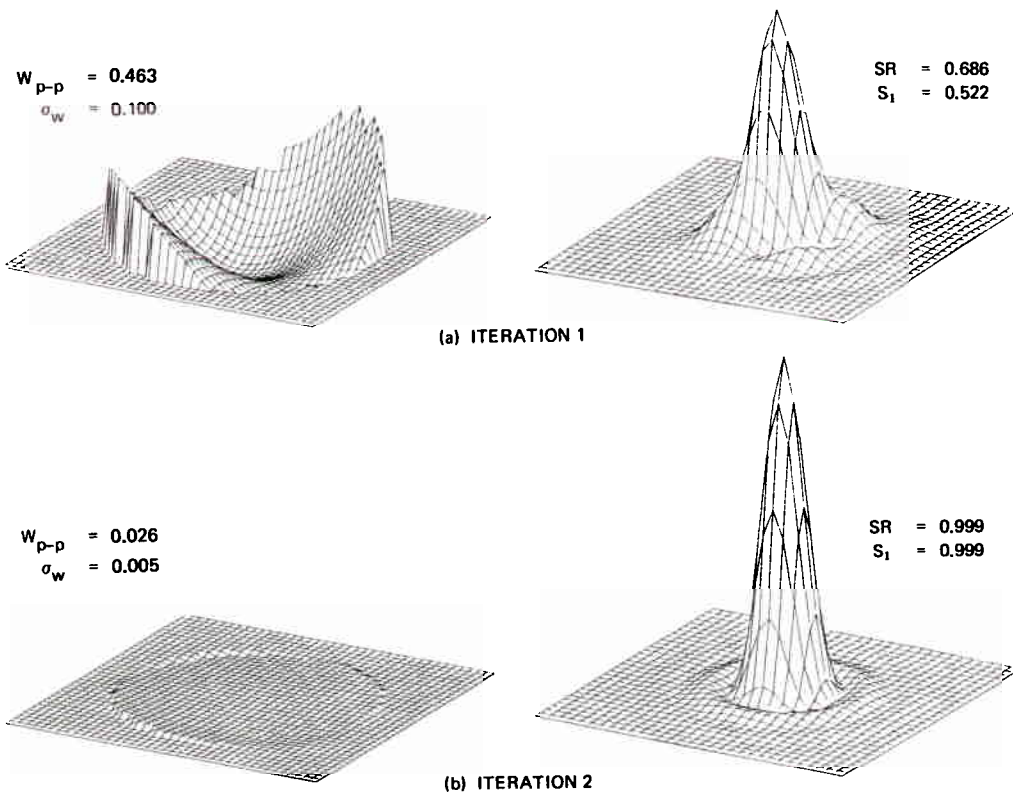


Figure 3. Phase retrieval using image sharpness function S_1 . The residual wavefront errors and the corresponding images after each iteration are shown.

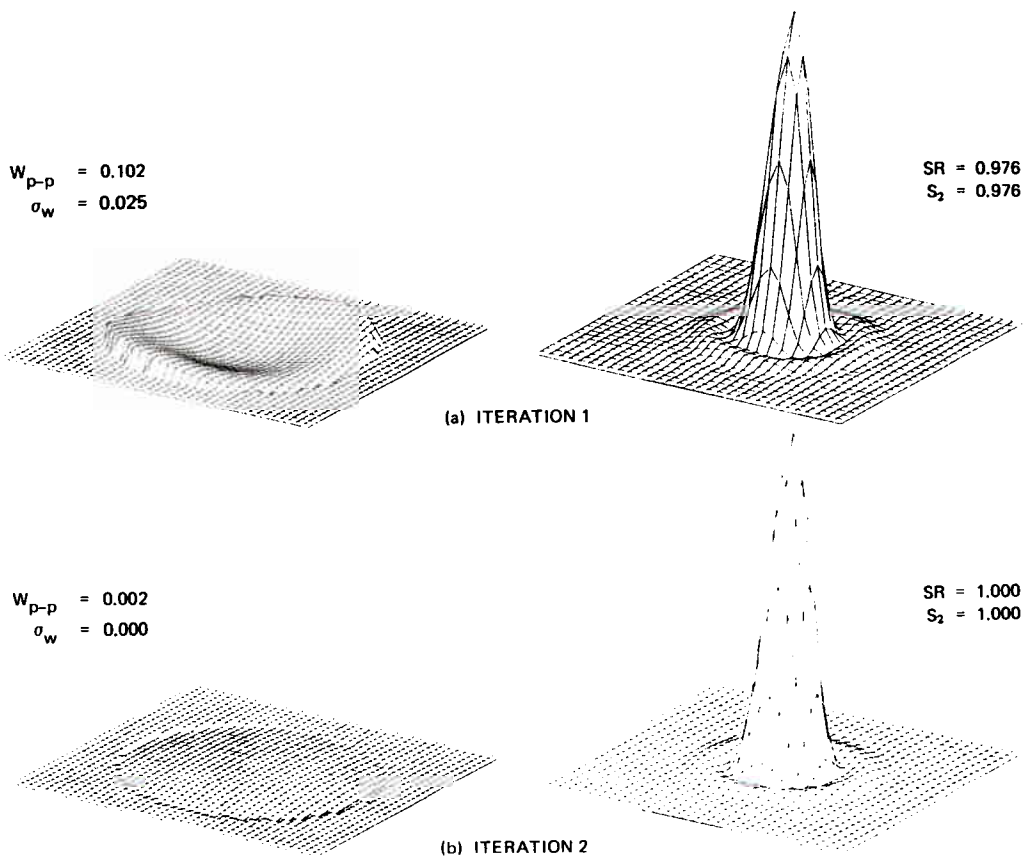


Figure 4. Phase retrieval using image sharpness function S_2 .

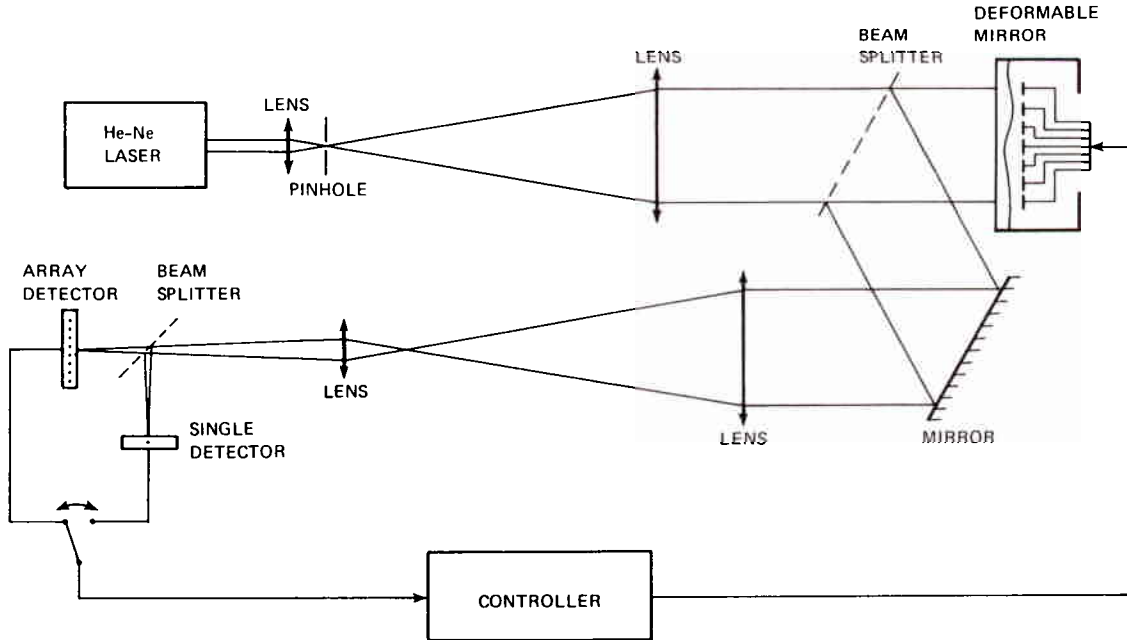
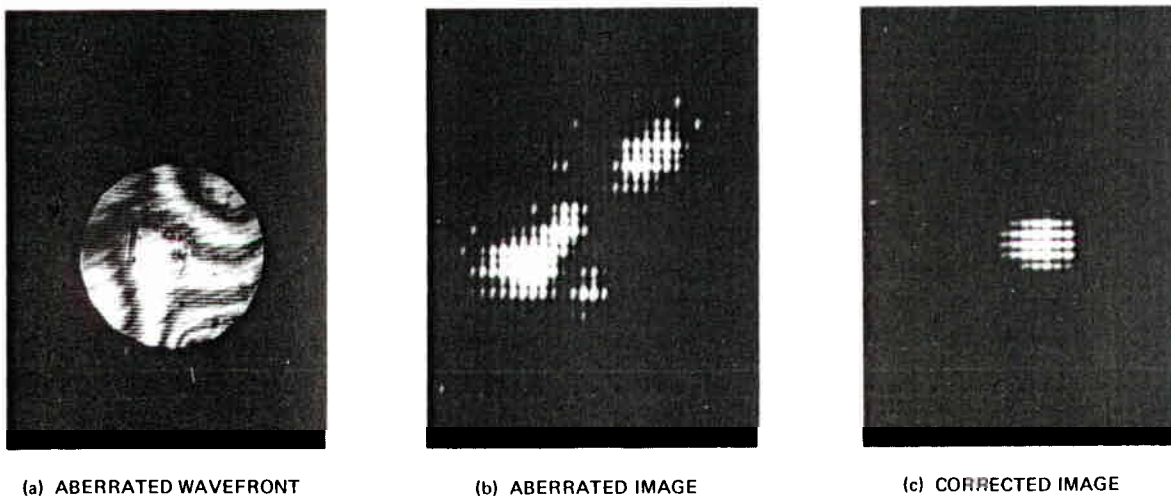


Figure 5. Schematic of the laboratory setup for adaptive correction of aberrated images.

the figure is such that it gives the interference fringes shown in Figure 6a. These fringes also include any errors in the rest of the optical train. The f-number of the imaging optics, which has a circular pupil, is approximately 600. The image as observed by a 32×32 photodiode array (supplied by Reticon Corporation), with center-to-center spacing of $100 \mu\text{m}$ between two adjacent photodiodes, is shown in Figure 6b. This array with its associated processor was also used to measure the sharpness function S_1 . An appropriately sized single detector was used to measure the value of the sharpness function S_2 .⁵ A digital controller addresses the actuators to deform the mirror in various Zernike modes. An example of a corrected image obtained by addressing six Zernike modes is shown in Figure 6c. These modes consisted of defocus ($n = 2, m = 0$), two astigmatisms ($n = 2, m = 2$), two comas ($n = 3, m = 1$) and spherical aberration ($n = 4, m = 0$). No observable difference between the quality of the images corrected by using sharpness functions S_1 and S_2 was obtained.



(a) ABERRATED WAVEFRONT (b) ABERRATED IMAGE (c) CORRECTED IMAGE

Figure 6. Adaptive correction of an aberrated image using sharpening.

Applications

The image sharpening technique described here is applicable to many problems where adaptive optics is needed. These include deformable high-energy laser (HEL) systems, thermal blooming, imaging through turbulent media, and disturbed large optical systems. Some of the HEL systems require adaptive optics due to all of these factors. The optical elements (e.g., mirrors) of an HEL system distort due to the high-power densities of the laser beam. We have shown⁶ that for circularly symmetric beams and an on-axis target, most of the thermally induced distortion is defocus with a small amount of spherical aberration. For an asymmetric beam and an off-axis target, tilt, coma, and astigmatism will also be introduced. Thus, for the thermally introduced aberrations of the system, correction of a few Zernike modes will be adequate.

For an HEL beam propagating through the atmosphere, depending on its power density, the refractive index of the atmosphere can change significantly and thus alter the phase distribution across it. This phenomenon, called thermal blooming, can severely degrade the target-plane irradiance distribution. However, by preaberrating the beam (e.g., with a deformable mirror), the phase errors can be compensated in many situations.

The atmospheric turbulence can not only degrade the target-plane irradiance distribution, but it can also degrade the image of the target observed at the HEL system. In fact, atmospheric turbulence can degrade any imagery encountering it. The time-averaged variance of aberrations introduced by Kolmogoroff atmospheric turbulence is given by⁷

$$\sigma_t^2 = 0.0261(D/r_0)^{5/3} \lambda^2 \tag{6}$$

where D is the pupil (beam) diameter, and r_0 is a characteristic length of the atmospheric turbulence.⁸ If the wave aberration caused by atmospheric turbulence is decomposed into an infinite set of Zernike modes, the reduction in variance of the aberration after correction of the first J modes is given by

$$\sigma_c^2 = \sum_{j=2}^J \langle a_j^2 \rangle \tag{7}$$

where, the time-averaged variance of a modal aberration is given by

$$\langle a_j^2 \rangle = 0.0192 \frac{(n+1)\Gamma(n-5/6)}{\Gamma(n+23/6)} (D/R_0)^{5/3} \lambda^2, \quad j \geq 2 \tag{8}$$

In Eq. (8), $\Gamma(\cdot)$, is the gamma function. The mode with $j = 1$ represents a uniform phase error across the pupil and therefore does not contribute to the aberration variance. The relationship between the indices n, m, and j is given in Table 2. Note that the variance of a modal aberration with a given value of n depends on n but not on m. Thus, all modes that have the same value of n but different values of m contribute equally to the aberration variance.

Table 2. Relationship between indices n, m, and j. (Note that for every nonzero value of m, there are two j values corresponding to the modes with cos θ and sin θ dependence.)

n	m	j
0	0	1
1	1	2,3
2	0,2	4,5,6
3	1,3	7,8;9,10
4	0,2,4	11;12,13;14,15
5	1,3,5	16,17;18,19;20,21
6	0,2,4,6	22;23,24;25,26;27,28

The standard deviation of the residual wave aberration after correction of the first J modes is given by

$$\sigma_J = (\sigma_t^2 - \sigma_c^2)^{1/2} \tag{9}$$

ADAPTIVE OPTICS WITHOUT WAVEFRONT SENSORS

Figure 7 shows how σ_J varies with J . It is clear that the first few modes contain a large fraction of the error. The reduction in error per mode decreases as the mode number increases. Thus, in situations where correction of a small number of modes gives an acceptable level of correction, the modal technique is very attractive. For example, if $\sigma_J \lesssim \lambda/10$ is acceptable, then for $D/r_0 \lesssim 5$, $J \lesssim 15$. The first 15 Zernike modes include all the aberrations up to the fourth order.

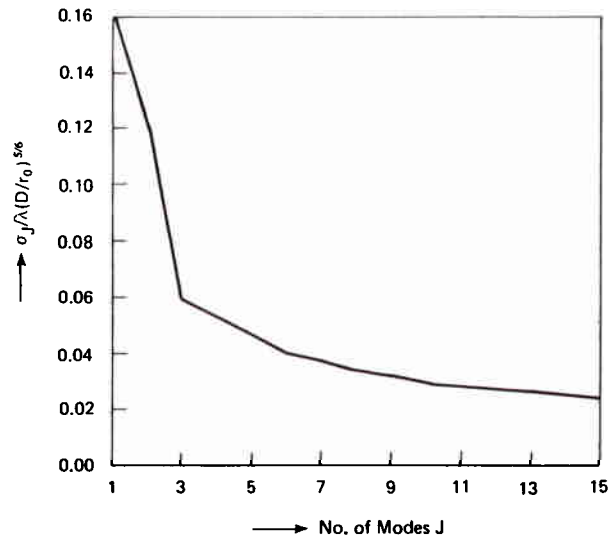


Figure 7. Variation of σ_J with J . (Note that the first mode, which represents uniform phase error across the pupil, does not affect the aberration variance.)

Large optical systems, especially the ones for space applications, use lightweight mirrors to reduce the weight and material cost. These lightweight mirrors are flexible and therefore deform when the system is disturbed. However, again most of their distortion is made up of the first few Zernike modes. Thus, the modal adaptive optics described herein are applicable to many situations of practical interest.

Acknowledgment

The work reported herein was performed under internal funding at The Charles Stark Draper Laboratory, Inc. The authors gratefully acknowledge the help and encouragement of personnel at the Rome Air Development Center. The hardware for the experimental work was developed under the direction of W. P. Curtiss of The Charles Stark Draper Laboratory, Inc.

References

1. Muller, R.A., and A. Buffington, "Real-Time Correction of Atmospherically Degraded Telescope Images Through Image Sharpening", *J. Opt. Soc. Am.*, Vol. 64, pp. 1200-1210, 1974.
2. Welling, P.A., Optimization of Image Sharpness in an Adaptive Optical System, Thesis, Massachusetts Institute of Technology, 1978. This reference contains early work on the development of the algorithm.
3. Born, M., and E. Wolf, Principles of Optics, 5th ed., (Pergamon, New York, p. 464, 1975).
4. Grosso, R.P., and M. Yellin, "The Membrane Mirror as an Adaptive Element," *J. Opt. Soc. Am.*, Vol. 67, pp. 399-406, 1977. See also, M. Yellin, "Using Membrane Mirrors in Adaptive Optics", *Proc. SPIE*, Vol. 75, pp. 97-102, 1976.
5. Buffington, A., F.S. Crawford, R.A. Muller, A.J. Schwemin, and R.G. Smits, "Correction of Atmospheric Distortion with an Image-Sharpening Telescope", *J. Opt. Soc. Am.*, Vol. 67, pp. 298-303, 1977. A one-dimensional analogue of our experiment is described in this reference.
6. Mahajan, V.N., and J. Govignon, "Computer Simulation of a Large Adaptive Optical System", *Proc. SPIE*, Vol. 72, pp. 439-451, 1979.
7. Noll, R.J., "Zernike Polynomials and Atmospheric Turbulence", *J. Opt. Soc. Am.*, Vol. 66, pp. 207-211, 1976.
8. Fried, D.L., "Statistics of a Geometric Representation of Wavefront Distortion", *J. Opt. Soc. Am.*, Vol. 55, pp. 1427-1435, 1965.